Available online at www.sciencedirect.com
ScienceDirect
Comput. Methods Appl. Mech. Engrg. 314 (2017) 473–493
Computer methods in applied mechanics and engineering
www.elsevier.com/locate/cma

Computational modelling of the respiratory system: Discussion of coupled modelling approaches and two recent extensions

Christian J. Roth, Lena Yoshihara, Mahmoud Ismail, Wolfgang A. Wall*

Institute for Computational Mechanics, Technical University of Munich, Boltzmannstrasse 15, 85748 Garching b. München, Germany

Available online 18 August 2016

Highlights

- Advanced coupled models of the respiratory system are introduced and discussed.
- We focus on the essential interaction between flow and deformation in the lung.
- Possible areas of application are provided to the reader for each model.
- Presented models are validated against regional and dynamic clinical measurements.
- Gas exchange on a realistic airway and vascular tree is derived for the first time.

Graphical abstract

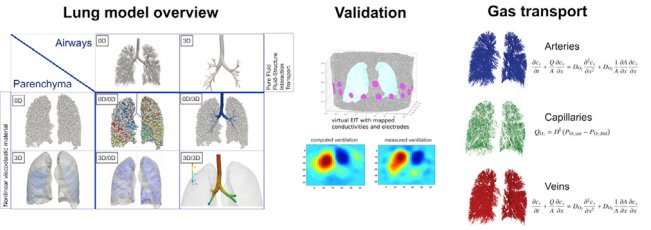

Abstract

In this article we present advanced computational models of the respiratory system with a special focus on approaches that are able to tackle the interaction between flow and tissue components which is necessary to accurately represent the underlying physics of the lung. We review complexity of this new generation of so-called coupled models and present strategies for sensible and target-oriented dimensional reduction. From this inherent complexity it becomes clear that there is no "one-size-fits-all" approach in the modelling of respiratory mechanics but one has to choose from a variety of different concepts to solve the problem at hand. We present four suitable coupled approaches introducing their underlying modelling idea and assumptions, their novelty against previous methods, possible scenarios of application, and limitations in a clinical practise. The quality of presented lung models is extended via regional validation against clinical measurements. This validation is performed using temporal highly resolved electrical impedance tomography monitoring. This detailed and for the first time dynamic regional validation generates further

* Correspondence to: Institute for Computational Mechanics, Technical University of Munich, 85748 Garching b. München, Germany.
E-mail address: wall@lnm.mw.tum.de (W.A. Wall).

http://dx.doi.org/10.1016/j.cma.2016.08.010

trust in the presented mathematically derived approaches. Finally the article closes with further steps towards simulation of gas exchange and local lung perfusion as the ultimate goal of respiratory modelling when ventilation is sufficiently understood.

Keywords: Respiratory mechanics; Fluid–structure interaction; Monolithic coupling; Reduced-dimensional modelling; Regional validation; Gas exchange

1. Introduction

The human respiratory system is a fascinating and at the same time a relatively young example of computational biomechanics and its application in medicine. Classical lung modelling approaches from a physiological/clinical perspective were until recently mainly limited to data-fitting of single compartment model parameters as e.g., described in [1,2] rather than based on a sound mathematical formulation of the underlying physics of the organ at hand. From a mathematical perspective, however, the lung consists of a complex network of branching compliant tubes spanning a wide range of scales and flow regimes from almost laminar diffusion dominated processes to highly turbulent and pulsatile flows. Further, at the terminal branches of the airway tree, flow enters into a sponge-like microstructure of lung tissue whose material behaviour is highly non-linear and whose topology is optimised for efficient gas exchange with small embedded blood vessels.

Recently, various efforts have been made in mechanical and mathematical modelling of the lung to (i) study isolated effects which are hard to assess in a subject *in vivo*, (ii) to advance medical imaging and functional diagnostics by incorporating computational models that are based on the underlying physics, and (iii) to finally assist in patient-specific treatment planning and optimisation.

Important steps towards a mathematical description of lung mechanics have been made by Bates [3] who built an inverse modelling approach with increasing complexity on mathematically sound formulations. The covered models range from single linear compartments to generalised multi-compartment models. A continuation of this concepts can be found in the work by Maury [4] who took up the idea of lumped compartments and describes the extension towards the lung as a resistive tree — an idea that has been proposed by many researchers in the respiratory field [5–9]. Further, the solution of the full Navier–Stokes equations for fluid flow is pictured from a very mathematical perspective. In fact, the most popular group of computational respiratory models consists of very detailed and computationally demanding fully resolved pure fluid representations of the respiratory system or parts thereof. This mainly includes solutions of the three-dimensional Navier–Stokes equations on rigid airway geometries [10–18]. As an approach to at least mimic the real fluid–structure interaction effects, approaches have been published that move the fluid domain using information from medical imaging data or other assumptions that overlay a known displacement field to the fluid domain, possibly denoted as “moving fluid” models [19–21]. The fully resolved fluid models are often used for investigating flow patterns in the lung such as vortices or jets, and for quantifying particle deposition or drug delivery in the upper and lower airways [22–24]. Due to the high complexity of such models, often only parts of the respiratory system have been investigated omitting essential effects in the entire organ.

However, a consistent and physiologically realistic representation of respiratory mechanics does not restrain to investigations in purely fluid mechanical or structural aspects, as the physics of the lung is governed by the interaction of the two fields. Actually, the way the human lung works is only possible due to deformation of the associated muscles, the lung tissue and the airway tree. Tissue properties and local deformations clearly influence airflow and transport processes e.g., of aerosols and gas exchange. Further, the investigation of processes during expiration requires a storage possibility for inhaled volume and there is actually only a very little number of studies available in respiratory mechanics which are able to simulate expiration.

Therefore, in this work we focus on the realisation of *coupled* models in respiratory mechanics which consistently incorporate the interaction between different fields and scales present in nature. The resulting next generation of respiratory models consists each of a Newtonian fluid and a non-linear viscoelastic structural domain. The concept of dimensional reduction, which is very successfully applied e.g., in models of the circulatory system, is introduced for the lung with its specific requirements. From this complexity it becomes clear that there is no “one-size-fits-all” approach possible, but one has to choose from a variety of available computational models to find the best solution strategy for the problem to be solved. We introduce four suitable models with different levels of complexity and

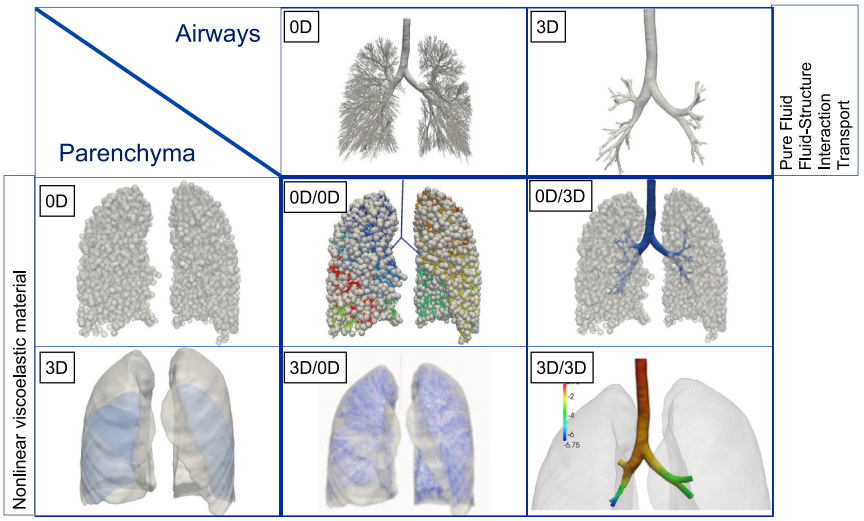

Fig. 1. Lung model overview. Each of the four coupled models consists of conducting airways and lung parenchyma. Each of these two building blocks can either be realised as fully resolved field denoted as *3D* or as a reduced-dimensional representation denoted as *0D*.

computational requirements. Each model is clearly motivated in its assumptions, encompassed to previously existing approaches, briefly sketched in its formulation and discussed in its applicability for possible areas of research at hand. This part of the article can be seen as a logical continuation of overviews and discussions of modelling ideas as given in Bates [3] and Maury [4] including current achievements published in the field.

In the second part of the paper, two possible extensions of the presented respiratory models are discussed. First, a validation approach for regional airflow in a subject *in vivo* is presented as a computational realisation of the clinically used electrical impedance tomography (EIT) monitoring. Second, a further step is made from regional ventilation towards gas exchange and the first investigations in perfusion of the lung based on a patient-specific circulatory tree. This part of the article gives a summary of the current state of the art in validating respiratory models and provides possible directions for further research in this particular field of computational biomechanics.

2. Coupled computational models of the respiratory system

In the subsequent section, various coupled approaches in respiratory mechanics will be introduced and discussed as presented in Fig. 1. Starting from the most general (and complex) fully resolved *3D* models for conducting airways and lung tissue, successively further assumptions will be reviewed that allow simplification towards easier and computationally cheaper tree-like *0D* representations still accurately representing the underlying physics. A specific focus will be put on the interaction between airflow and tissue behaviour in terms of consistent coupled computational models for respiratory mechanics. Possible fields of application will be given for each model to guide the reader towards the best solution strategy for a given clinical or research question.

We start with the most complex model in our table. This is in contradiction to the classical engineering approach of starting simple and getting more complex if needed. However, in our opinion this is well justified since, amongst others so little can be measured in the respiratory system that often the only way to check certain assumptions or effects is given by the most advanced models.

2.1. Fully resolved three-dimensional lung model (3D/3D)

2.1.1. Motivation and model description

The first and most general approach in our overview is motivated by the fact that certain questions in respiratory mechanics require both a fully resolved deformable three-dimensional fluid domain and a realistic three-dimensional structural representation of the lung. However, these two fields are not behaving independently from each other but are coupled in its action and reaction. First, the embedding of the tree in surrounding lung tissue provides realistic additional strength against local collapse and hyperinflation of both airways and lung tissue. Secondly and even more

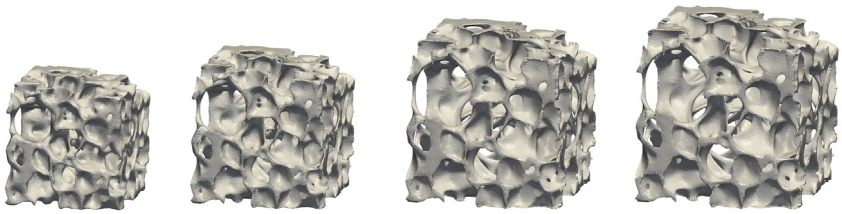

Fig. 2. Exemplary inflation states for incompressible lung tissue doubling the enclosed volume of air in the parenchyma block while the volume of tissue remains constant.
Source: Geometry taken from [30].

important, flow throughout the conducting airways is naturally coupled to regional inflation of the respiratory part of the lung.

Therefore, a core element and the main novelty of the approach denoted as *3D/3D* compared to previous fluid, moving fluid, and fluid–structure interaction (FSI) approaches of the bronchial tree [25–28] is the mutual volumetric coupling between fluid flow and regional deformation of lung tissue [29]. We resolve conducting passages of the tree only as far as necessary for the current investigation and model all downstream passages as a kind of homogenised solid domain of lung tissue containing alveolar walls, small airways and blood vessels. This homogenised tissue is in the following referred to as *parenchyma*. The introduced volumetric coupling approach respects inflation of a tissue region dependent on the fluid flow leaving the associated tree outlet. Vice versa deformation of a tissue region e.g., via contraction of the associated muscles, creates a volume flow at the current fluid outlet and drives airflow throughout the tree. This is remarkable as apart from a zero-pressure at the mouth/nasal cavity there is no need to impose additional boundary conditions to the deformable fluid domain for such a scenario.

The underlying well justified assumptions for this and for all following models are that air can be seen as a Newtonian fluid and the flow as incompressible in the physiological regime (Mach number below 0.2 [31]). Further, airway walls and small blood vessels in the parenchyma can be seen as incompressible due to their high water content and the well-grounded assumption that water can be seen as incompressible at the timescales relevant in respiratory mechanics. Therefore, all air which leaves the compliant airways and enters a region of lung tissue has to increase air spaces therein, i.e., the pores of the sponge-like micro-structure (see Fig. 2 for different exemplary states of parenchymal inflation). The transition from a fully-resolved airway to the homogenised parenchyma can be modelled without additional transition zone and fully-resolved airways and homogenised parenchyma are directly coupled via the volumetric constraint [29]. In case the coupling is assigned at lower tree generations, an additional flow-dependent pressure term can be included in the coupling to account for the resistance of all downstream airways that are not fully-resolved.

The realisation of this volumetric coupling within a framework of classical fluid–structure interaction is presented in Fig. 3 and will be briefly sketched for a four outlet case in the following. Airflow in the deformable fluid domain Ω^F is governed by the incompressible Navier–Stokes equations in Arbitrary Lagrangian–Eulerian (ALE) formulation. The deformation of lung tissue in the homogenised lung tissue Ω^S is described via the non-linear elastodynamics equations. A classical FSI interface denoted as Γ is used to represent the interaction between airflow and deformation of the airway wall. For each pictured outlet of the fully resolved compliant airways $\hat{\Gamma}^i$ a volumetric constraint is introduced that couples fluid flow Q^i to the volume change ΔV^i of the regions bounded by $\tilde{\Gamma}^i$ in a defined time-interval. Obviously, the number of outlets and homogenised solid domains is arbitrary and depends on specific requirements of the question at hand. For more details on the enforcement of the constraint and detailed solution of the resulting system of equations of the *3D/3D* model the reader is referred to [29,32].

2.1.2. Discussion and example applications

In brief, the model presented as *3D/3D* in our overview is an FSI problem extended by the idea that all fluid flow that enters or leaves an outlet of the deformable fluid domain has to change the volume of the associated parenchymal region inducing deformation.

The advancements compared to pure fluid and moving fluid are apparent. The volumetrically coupled *3D/3D* model induces a consistent deformation of the fluid and structural domains which is governed by the current flow characteristics and not prescribed from additional information such as imaging data recorded under different or

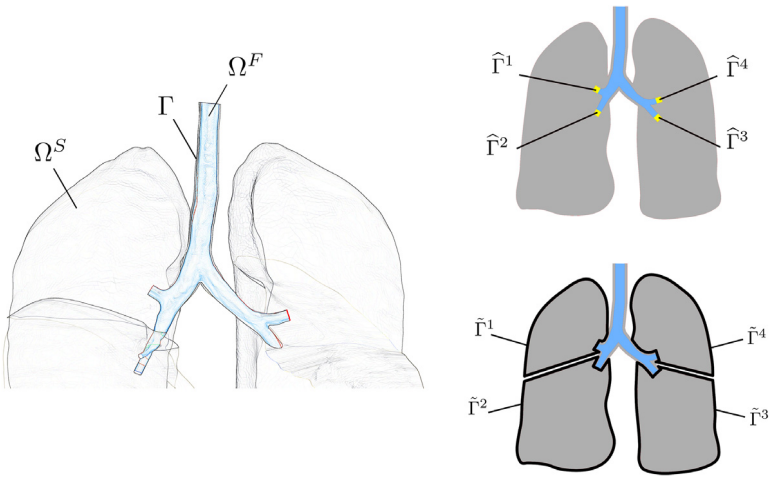

Fig. 3. Model schematic for the approach denoted as *3D/3D*. The deformable fluid domain is denoted as Ω^F, the structure as Ω^S and the interface for classical fluid–structure interaction as Γ. The novel volumetric coupling is realised between the fluid outlets $\hat{\Gamma}$ and the structural domains bounded by $\tilde{\Gamma}$. All fluid that leaves an outlet $\hat{\Gamma}$ has to increase the volume of its associated region $\tilde{\Gamma}$. For easier display the sketch is exemplified for the main bronchi leading to the five lobes of the lung (left). For the definition of the boundaries of the structural domain a slice of the lung is used where only four lobar bronchi are visible (right). The marked boundaries correspond to the anatomically correct boundaries of the single lobes obtained from the CT scan.

ambiguous flow conditions. Further, correct boundary conditions are applied at the last fully resolved generation of airways of the deformable fluid domain. The other way round, local tissue deformation induces the correct airflow in the compliant airways without any need of prescribing additional boundary conditions to the fluid. Thereby, physiologically reasonable kinematic constraints can be imposed on the 3D parenchyma model. The role of the thoracic cage and the respiratory muscles can e.g., be taken into account using nonlinear spring-dashpot combinations orthogonal to the deforming lung surface. This allows consistent expiration based on the previously inspired local volume in each branch. We might annotate that flow entering the domain at each branch does not have a prescribed velocity profile, but the profile is allowed to develop under the current flow conditions. This requires, however, stabilisation of backflow into the domain [33,34].

The point of volumetric coupling is to be chosen carefully for each setting. Full resolution of a further generation of airways in the tree doubles the number of outlets and significantly increases complexity and computational cost. If this, however, does not come along with simultaneous knowledge of material parameters or sufficient resolution of imaging data for geometry generation, a further uncertainty is introduced which needs to be taken into account or could considerably corrupt results and derived conclusions. Previous studies have shown that turbulent effects in the trachea abate after the 3rd–4th generation [17]. At the level of the 7th generation, the associated tissue regions correspond to single lung segments with an approximate size of 20–30 mm. This is usually sufficient for most studies to resolve heterogeneity between different tissue regions obtainable e.g., from imaging data.

With this considerations, one proposed area of use for the *3D/3D* model is for example simulation of a fully-resolved strain state during mechanical ventilation of heterogeneous lungs. The fully resolved model is able to quantify volumetric and isochoric strain components which can be transferred towards loading of the micro-scale using a multi-scale coupling approach [35]. This is especially interesting in understanding of the onset and progression of diseases such as ventilator-induced/ventilator-associated lung injury (VILI/VALI) which are assumed to be linked to excessive strain and repetitive collapse and opening of alveolar structures [36]. Further, it is possible to drive respiration by local tissue deformation acquired e.g., from a time series of imaging data over the breathing cycle [37]. In the same course the model is able to deduce local mechanical tissue properties in an inverse sense by simulating distortion during inflation and deflation and comparing with imaging data. By this means suspicious tissue regions such as cancerous areas might be identified. Prediction and tracking of local tumour movement during quiet breathing is also conceivable and provides valuable information for radiation therapy planning.

The generality of this modelling approach, the interaction between different physical fields and the possible high resolution of the domains, however lead to computational costs that limit the applicability in a real-time clinical setting. Although efficient solution strategies have been developed for this problem and show almost optimal scalability

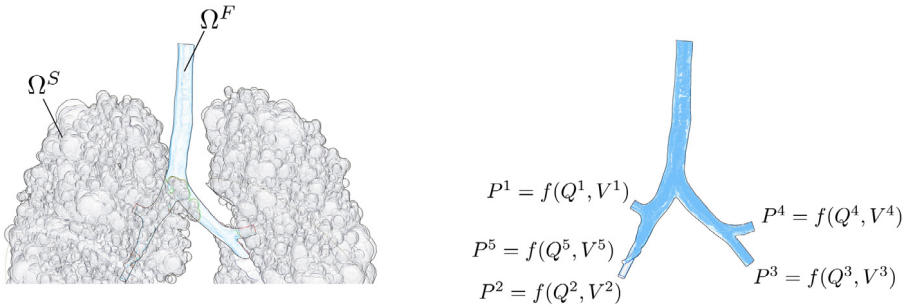

Fig. 4. Schematic for the *0D/3D* model consisting of a fully resolved deformable fluid domain Ω^F and a reduced model of lung tissue Ω^S realised as flow- and volume-dependent non-linear boundary conditions $P = P(Q, V)$. For easier display the sketch is exemplified for five outlets only.

on high performance computing platforms [32], a single breath of the model can take up to more than one day of computing time. One possibility that builds upon availability of this general approach is the investigation of simpler models which might show similar results in certain applications but significantly reduce computing time. In the following, we will now introduce such simplified models for different applications in respiratory mechanics. We might, however, keep in mind that evaluation of their performance for novel applications might require learning steps from the fully resolved model.

2.2. Reduced-dimensional structure and fully resolved three-dimensional fluid (0D/3D)

2.2.1. Motivation and model description

A first simplification of the previously described model is applicable if a fully resolved fluid domain (rigid or coupled with surrounding flexible airway walls) is required, while a three-dimensionally resolved structural representation can be omitted. At the terminal ends of a fully resolved deformable fluid domain, appropriate boundary conditions have to be defined representing the omitted lung tissue [4,7,16]. Here, the terminal ends of the fully resolved tree are defined by the current region of interest, the available computational resources, or simply by the resolution of available imaging data. The effect of tissue inflation and the resistance of the airways further downstream generate dynamic pressures at the outlets which are clearly different to the zero-traction or constant pressure ones which are often used by the biomechanics community [14,15,22,23,28]. Further, there has to be a storage possibility for outflowing volume during inspiration at each outlet which must allow flow to re-enter the domain for consistent representation of expiration without prescription of intransparent patient-specific boundary conditions [20].

Therefore, the tissue region associated to each outlet is modelled via a non-linear pressure boundary condition. Depending on the size of the tissue region and its material properties, a non-linear pressure–volume relationship $P = P(V, Q)$ can be derived to represent the regional compliance at each outlet (see Fig. 4).

This derivation can for example be realised from detailed experimental and numerical data on an alveolar duct model [38–40]. Alternatively, regional functional diagnostics can be included and it is generally possible to prescribe any linear or non-linear function $P = P(V, Q)$ that represents the known regional compliance at each of the outlets. A generalised Maxwell model which we use as a pressure–volume relationship in this context, has been shown to represent patient behaviour in the entire range of physiological pressures [9].

One assumption which is inherent in using a functional relationship for flow-dependent outlet pressures is that there are no recirculation zones occurring across the fluid outlets. We also assume that tree elongation induced by inflation of lung tissue is small [41]. Thus, there is no significant distortion of the deformable fluid domain especially in terms of branching angles that could alternate recirculation zones at bifurcations within the domain and associated particle flow during respiration. We might annotate that the radial expansion of the airway tree, which leads to different cross sections during in- and expiration or in cases of bronchoconstriction, can be included in this approach via respecting fluid–structure interaction with flexible airway walls. In such studies the stabilising effect of surrounding tissue can e.g., be modelled via simple springs with the stiffness of lung parenchyma attached to the outside of airway walls.

The novelty of the *0D/3D* concept is characterised by two core effects: First, a computation of correct pressure levels at the outlets of the compliant airways is enabled. Second, fluid volume leaving the deformable domain can be

stored and re-enter the domain for consistent modelling of expiration again making use of sophisticated stabilisation techniques [33,34]. Without such a storage possibility it is not known how much air flows into the domain from different outlets and additional assumptions have to be included for modelling expiration. This is of particular importance in the relevant case of heterogeneous lungs. This is also the main difference to previously used Windkessel or impedance models [16] which might provide a correct pressure niveau but lack the possibility of storage.

The underlying mathematical formulation of airflow is equal to the previous model and governed by the incompressible Navier–Stokes equations possibly including FSI. The lung tissue region is respected via the non-linear relationship between the flow Q and the volume V of the attached region to be modelled as integrated volume over time starting from the fully expired state. One particular established concept here is to compute an equivalent resistance R_{eq} for the airway tree further downstream the current outlet and combine this equivalent resistance with an averaged compliance C of the lung tissue in question. To avoid iterative solution of the boundary pressure and the flow leaving the compliant airways at the current outlet, a linearisation of the pressure boundary condition can be included in the Navier–Stokes equations and directly be solved within the Newton procedure of the fluid problem. For more details on this computationally efficient approach, the reader is referred to [33].

2.2.2. Discussion and example applications

In summary, the *0D/3D* model is a classical fluid or FSI problem extended by a nonlinear boundary condition for the outlet pressure dependent on current flow into and volume of the tissue to be modelled. For efficiency, the boundary condition is linearised within the system of equations of the fluid/FSI problem and can be solved within the same Newton step, i.e., no further iteration loop is needed for computing the boundary pressure.

We put the coupling of a fully resolved deformable fluid domain with resistive airway trees also in this model category as it shows basically the same effect on the deformable fluid domain. Whether such models are able to model expiration depends on availability of storage capacity at the terminal ends of the tree. This applies to [7,13,18,24,42–44].

The novelty against previous approaches seems small, however, it has great impact in the field of respiratory biomechanics. Without a representation of lung tissue, fluid would mainly flow through outlets with large diameter as their resistance is small. However, this large airways might lead to tissue regions with increased stiffness or collapse which significantly hinders incoming airflow. Therefore, ventilation of diseased regions would be over-estimated. Also, transport of curative aerosols to rehabilitate original lung function in such regions would be overrated. Further, one needs a storage capacity for lung volume during inspiration which can re-enter the domain during exhalation. This is also the reason why classical Windkessel or impedance models have to be extended, as they are not able to store the entire outflowing volume and would lead to mass-loss over the breathing cycle.

In fact, the lung is the only organ in the human body which is passed through in two directions. Interesting phenomena have, however, so far mainly be investigated during inspiration due to lack of appropriate boundary conditions. Now, also studies of phenomena which occur during the phase of flow reversal or even after a few cycles are possible. This might lead to totally different patterns of particle deposition or carbon-dioxide clearance than assumed today.

In general the *0D/3D* approach is recommended to study flow in larger airways that are stiff enough and/or for small tidal volumes that do not cause too much deformation and distortion of the bronchial geometry. Next to several examples presented in the introduction [10–18], many investigations in transitional and turbulent flow phenomena [45–48] and transport [22–24,42,49] can profit from this type of model. Studies, which are claiming that FSI is not required for the bronchial tree have to be checked carefully [28]. If such statements are made without correct representation of outflow boundaries, dynamic pressure changes during respiration are purely based on flow resistance and will be under-estimated. Consequently smaller pressures under-estimate tree deformation in radial direction.

2.3. Fully resolved three-dimensional structure and reduced-dimensional fluid (3D/0D)

2.3.1. Motivation and model description

Analogously to the previously described model also a simplification of the deformable fluid domain is possible while the structural part of the lung remains fully resolved.

This can be realised via the concept of dimensional reduction of the compliant airway segments well known and widely used e.g., in cardiovascular mechanics [50,51]. Under certain assumptions (see below), the velocity profile can

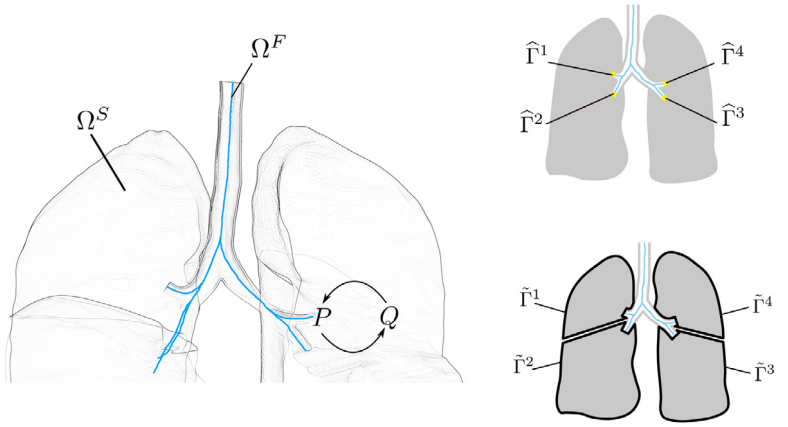

Fig. 5. Schematic of the *3D/0D* model with a fully resolved lung tissue and a reduced-dimensional formulation for the compliant airways indicated as centreline. The pressure P and airflow Q at the fluid outlets $\hat{\Gamma}$ are coupled to the inflation of the associated structural regions denoted as $\tilde{\Gamma}$. For easier display the sketch is exemplified for four of the five lobar bronchi visible in this lung slice only (see also Fig. 3). The marked boundaries correspond to the anatomically correct boundaries of the five lung lobes visible in this lung slice.

be integrated in radial and axial direction towards a zero-dimensional (*0D*) formulation. This reduced-dimensional formulation is essentially a relation between pressure and flow in an airway segment and can be used to compute the pressure drop along the airway tree for a certain flow. The other way round, resulting flow can be evaluated for a given pressure difference between inlet and terminal ends of the tree. Outlet pressures and flows are further coupled to the volume changes of the associated structural regions and thus airflow is again linked to structural deformation (see Fig. 5).

The novelty of this approach lies in the availability of an efficient reduced-dimensional flow model with all benefits of a fully resolved structure. This covers a fully-resolved and local quantification of stresses and strains in the parenchyma. Further, an effect known as interdependency [52] is inherent in all fully resolved structural models. Physically, interdependency is the interaction between neighbouring air spaces which share a common alveolar wall. If single air-spaces expand or shrink, this influences their neighbours towards shrinking/expansion such that there is no overlap or gap between them. Interdependence is thus an important concept to add stability to the lung against local over-inflation or collapse by the stiffness of surrounding tissue. Finally, the *3D/0D* model offers a possibility to prescribe imaging-based regional deformation of lung tissue to a fast reduced-dimensional flow model.

The derivation of such a reduced-dimensional set of equations requires some assumptions. Flow is assumed to be axisymmetric, fully developed, and all airways are seen as straight. Then the velocity profile can be integrated in radial direction towards a one-dimensional (*1D*) formulation. Further, as the pressure wave speed inside a compliant airway is up to three orders of magnitude higher than actual flow velocity [7], the dynamics of wave propagation can be omitted if one is interested in an approximate solution on the timescale of fluid flow. On this timescale, the pressure wave has already travelled through the entire airway segment and therefore, following the derivation in [51], the *1D* formulation can be further integrated in axial direction towards a model known as *0D*. This *0D* formulation essentially offers a relationship between pressure drop along and flow through an airway segment. We might annotate that the *0D* approach does not restrict to pure Poiseuille resistance models but can also contain the concepts of airway compliance and inertia of air, as well as viscoelastic behaviour of airway walls [7,9].

The coupling with the structure will be briefly explained following the idea of a partitioned scheme. Let us assume that a certain pressure is prescribed at the tracheal inlet. This induces a flow through the reduced-dimensional compliant airways and a resulting pressure drop across the tree. The resulting outlet pressure at $\hat{\Gamma}^i$ is then prescribed as a traction to the surface $\tilde{\Gamma}^i$ and induces a volume change of the region that is bounded by this surface $\tilde{\Gamma}^i$. This volume change $\Delta V/\Delta t = Q$ is then handed back to the reduced-dimensional tree outlet and adjusts the flow accordingly with a relaxation factor and the flow from the previous iteration. This procedure is repeated until computed pressure and flow are at equilibrium. Obviously, such models can also be solved in a monolithic way more or less as given e.g., in [29,32]. A similar approach that includes coupling of reduced-dimensional fluid with a poroelastic structure is given in [8].

2.3.2. Discussion and example applications

The model denoted as *3D/0D* is essentially a combination of pressure and flow computed from well-known reduced-dimensional fluid models with volume changes and tractions of a fully resolved structure or poroelastic medium.

This concept is valuable when mainly structural aspects of the lung are to be investigated. Here, the reduced-dimensional representation supplies a simple and computationally cheap solution of the fluid quantities and its effect on structural deformation/inflation.

It is important to mention that even though turbulence cannot be resolved with the reduced-dimensional fluid approach, the effect of turbulence can be modelled. This means that if the *0D* model detects an airway with a higher Reynolds number than those defined as critical for the straight tube ($\mathrm{Re}_{\mathrm{crit}} = 2300$) the resistance will be adapted following the approach by [7,53,54]. We might further annotate that it is also possible to gain further tree generations e.g., from a tree-growing algorithm introduced in the next section. This allows finer subdivision of the tissue structure in smaller compartments and higher resolution of heterogeneity as would be possible with the airway tree segmentable from imaging data. Finally, to account for kinematic constraints on the lung, additional contributions can be applied in form of additional tractions on the lung surface which would physiologically e.g., arise from the deformation of the thoracic cage and the diaphragm.

Possible areas of usage for such an approach are investigations of detailed strain states during mechanical ventilation. As e.g., VILI/VALI are predominantly influenced by structural stresses and strains [55], a reduction of the deformable fluid domain might be conceivable. Under the same aspects a full resolution of the deformable fluid domain might be negligible for diagnosis of regions with suspicious material behaviour or 4D-CT tumour tracking applications. The main benefit of this approach as compared to the *3D/3D* model are the associated computational costs. In comparison with the *3D/3D* model the *3D/0D* approach is approximately 10 times faster for the same patient-specific geometry and boundary conditions described in detail in [29].

2.4. Reduced-dimensional lung model (0D/0D)

2.4.1. Motivation and model description

The most efficient and reduced model is the one presented as *0D/0D* in our overview (Fig. 1). This approach combines a reduced-dimensional formulation for compliant airways with a functional relationship between pressure and volume of the terminal units of the tree. This is conceivable if no fully-resolved velocity profile is necessary for the current investigation and solely pressure and flow should be computed in the compliant airway segments. Further, on the structural side many cases only require the magnitude of regional strain while a detailed composition of isochoric and volumetric components is negligible. Then, a *0D* tree of compliant airways with up to 23 generations can be generated via a tree-growing algorithm [7,56] providing high spatial resolution for *0D/0D* modelling.

In fact many extremely efficient models in computational modelling of the respiratory system live from the fact that the airway tree is a well understood dichotomous branching structure. The branching patterns as well as diameter and length ratios are very well documented for humans [7,56–59] and for other species such as mice, which are often used in experiments [60]. This means that no segmentation of the entire tree is required to generate a patient-specific respiratory model. The hull geometry of the lung and the directional vector of the lobar bronchi are sufficient to generate a realistic coupled *0D/0D* model for each patient individually.

The assumptions for dimensional reduction of the deformable fluid domain are explained in Section 2.3 and are repeated briefly. The velocity profile of airflow is seen as axisymmetric, fully developed and airway curvature is neglected for velocity integration in radial direction. For further integration in axial direction the pulsatile character of airflow is omitted as pressure wave speed is up to three orders of magnitude faster than flow velocity [7]. On a timescale in which fluid flow is resolved, the pressure wave has already passed through the entire airway segment in one time step and pressure fluctuations can be averaged along the airway axial direction as described in [51]. These assumptions are perfectly valid under (patho-)physiological conditions and the *0D* compliant airways are able to reproduce the pressure and flow properties of a fully resolved *3D* patient-specific fluid domain as shown in [7]. Further, it is assumed that the behaviour of lung tissue at the terminal ends of the tree, i.e., of the alveolar ducts, can be represented via a functional relationship. Detailed experimental and numerical investigations on alveolar ducts are available in the seminal work by Denny and Schroter [38–40] and we have shown that our non-linear Maxwell model perfectly matches static pressure–volume and dynamic curves presented in these studies [9].

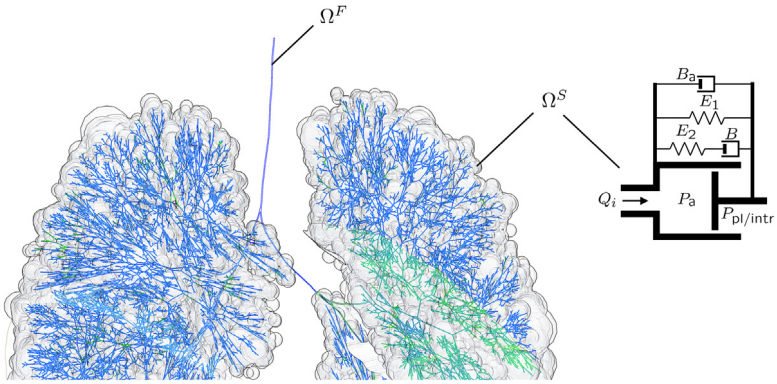

Fig. 6. Schematic of the model denoted as *0D/0D*. This model is composed of reduced-dimensional compliant airways Ω^F indicated by the centreline of the bronchial tree generated via a tree-growing algorithm. The non-linear acini Ω^S are represented via a Maxwell-model consisting of (non-)linear springs E_1, E_2 and dashpots B_1, B_2 that mimic the relationship between the pressure difference $P_a - P_{pl/intr}$ and flow Q_i into lung tissue.

One novelty compared to existing reduced-dimensional models [5,6,8] is the previously explained (see Section 2.3) ability to take into account and consistently model turbulence effects [7,53,54,61]. Further, the generation-dependent resistance model by van Ertbruggen [61] is only valid during inspiration. Therefore, the radius reduction of the convective ducts during expiration is respected via an additional equation for determination of airway radius dependent on the pressure difference across the wall and viscoelastic airway compliance. In the same course, airways are not only able to change its diameter but also to fully recruit and derecruit following the dynamic laws derived by the Bates group [62–64]. As a tissue model we use the non-linear Maxwell model from [9] which has been shown to be valid over the entire physiological pressure range. A final novelty overcomes the lack of tissue interdependence - a main objection against the usage of reduced-dimensional models so far. Recently, this concept has been proposed for reduced-dimensional lung models [9] to model volume-competition between inflating neighbouring acinar ducts resolving previous misconception [65].

Fluid flow in the deformable domain Ω^F indicated by the centreline of the tree in Fig. 6 is governed by the *0D* formulation for pressure and flow. Flow Q_i into the acinar ducts Ω^S is then described via the generalised Maxwell model consisting of (non-)linear springs and dashpots and is dependent on the pressure difference $P_a - P_{pl/intr}$. In case of an acinus that is in contact with the pleura, i.e., the hull contour of the lung, a pleural pressure P_{pl} is prescribed. In case the current acinus is located inside the domain it is surrounded by neighbouring acini and consequently an averaged interdependency pressure P_{intr} is used. Interdependency is then basically taken into account by linking external acinar pressures and thus propagate forces between neighbouring acini. Additionally, collapsed and open states for each airway are computed via virtual trajectories. A decision between fully open and closed state is dependent on current and previous airway inner pressure, the critical open/closing pressure and time constants for closure/reopening. For solving the fully problem, the “stiffness” matrices of airways and tissue are assembled into a single system matrix, a single solution vector containing the pressures P and a single right hand side containing the fluxes Q. A classical Newton method is then applied to solve the non-linear set of equations. For a more detailed derivation of the mathematical formulation and solution the reader is referred to [7,9,64]

2.4.2. *Discussion and example applications*

The last presented *0D/0D* model is essentially a dimensionally reduced relationship between pressure and flow in the compliant airways and in the viscoelastic acini equipped with all properties that are necessary to accurately describe the underlying physics of the lung. Extensions include interdependency, a literature-based thorax boundary condition, flexible airways able to collapse and reopen [64], and an acinar model that is valid over the entire physiological pressure range [9].

Such a model is often sufficient for answering clinical questions especially when considering the quality of input data. Errors in segmented geometries due to low resolution and contrast in medical imaging might e.g., introduce errors in velocity profiles such that only averaged flow remains as reliable quantity. Also, local pleural pressure measurements which are challenging [66] can corrupt a derivation of strain components and sometimes allow

only quantification of absolute magnitude. Further, time is a critical component limiting computation and detailed interpretation of fully resolved quantities in a clinical setting. Many more questions arise when trying to bring a computational model into a clinical setting, i.e. to bedside. An important one might be: "Do we compute something that is already contained as model input or can possibly never been validated in reality?", and we will try to provide an answer in the following section.

The described *0D/0D* model actually performs well in many of these points. It is in good agreement with fully resolved three-dimensional simulations of airflow [7] which underlines the quality of results in realistic settings. Further, the model is still built on solid mathematical ground and thus requires no extensive fitting as single and multi-compartments do. All important phenomena such as interdependence and recruitment or derecruitment are included and successfully tested in patient-specific examples or experimental animal studies [64]. This patient-specific case also shows that the *0D/0D* approach is 100–500 times faster than *3D/3D* for same patient. Further its predictive capability is verified against clinical measurements [67].

In retrospect, the *0D/0D* approach meets several points of motivation that have led to development of computational lung models. It (i) enables to isolate certain effects computationally e.g., by changing parameters such as peak ventilatory pressure and allows evaluation of resulting local ventilation. Second (ii) the model gives an additional insight into regional tissue aeration and mechanical strain distribution which is not obtainable from imaging data. Finally (iii) the model shows a predictive capability as it is not built upon extensive fitting of clinical measurements but can be validated against such data globally and regionally (see Section 3.1). Thereby pre-computation of certain therapy options can be performed and resulting optimal strategies can be applied to the patient only if the computationally prediction shows improved outcome. Inadequate or high-risk-high-reward settings do not have to be tested at a real patient.

Possible areas of application of the *0D/0D* approach are the investigation of VILI/VALI mainly because the *0D* compliant airways are comparably good as the *3D* and because regional strain magnitude is already an extremely valuable quantity compared to current clinical investigations [68]. Another application is the evaluation of collapse and the design of possible reopening manoeuvres *in silico* as one example for high-risk-high-reward manoeuvre. Further, this model is applicable as relatively robust basic approach for further gas-exchange models.

Potential directions for further research in this context might be the integration of patient-specific thorax boundary conditions and collapse and reopening computations in a realistic unsymmetrical patient-specific tree geometry investigating phenomena with high impact hypothesised previously [69].

2.5. Final remarks

In this chapter we presented four different models of the respiratory system which are derived from underlying physical principles and consistently represent the interaction between fluid flow and tissue inflation in the lung. We walked down the road from fully resolved towards simpler dimensionally reduced models introducing all necessary assumptions and resulting limitations. Finally, we end up with a coupled computational respiratory model (*0D/0D*), which is both fast to compute and reliable in its quality of clinical prediction. For a number of clinically relevant questions such models seem to be the most promising approach to deliver patient-specific regional pressure and flow quantities and to meet the challenge of optimising ventilation in a clinical setting.

The next chapter shows two recent extensions of this model, where the *0D/0D* model is subsequently equipped with an approach for extensive dynamical and regional validation against clinical measurements and used as a basis for investigations in gas transport and exchange.

3. Two recent extensions

3.1. A possible method of validation for advanced computational lung models

Advanced computational modelling requires rigorous validation. This statement is true even if the models in question are solely derived from basic physical principles such as the respiratory models proposed in the previous section, as well as for those existent in literature. However, such a detailed validation is often difficult. One reason is that many quantities that can be computed easily with models *in silico* are hard to assess in a subject *in vivo* or are not measurable at all. Investigations that would interfere with planned treatment, high radiation doses in

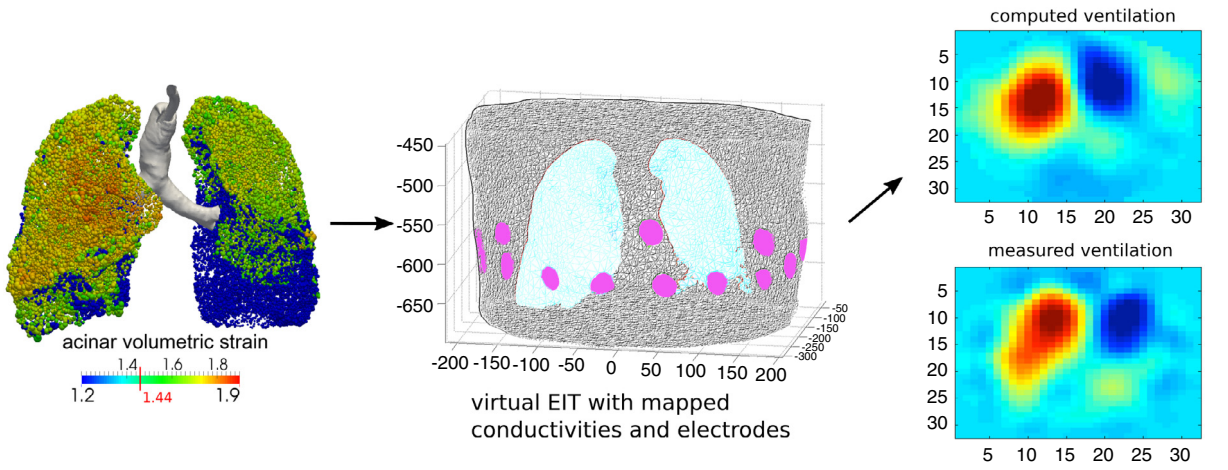

Fig. 7. Validation of computational lung models in terms of detailed dynamical regional ventilation using a virtual EIT module. Regional air content in terms of acinar volumetric strain is provided by the presented lung models (left). This regional air content is converted to regional conductivity and virtual EIT imaging is performed on the patient's real thorax with the marked electrode positions (middle). The computed virtual EIT voltages are reconstructed in the electrode plane and the image showing computed ventilation can be compared to the measured EIT image (right).

imaging or invasive measurements should not and cannot be realised in a clinical setting to cross-check results that are obtained from mathematical models. In a few cases, it also remains ambiguous which data have been used for model generation and thus are not allowed to be used for validation of actually something that has already been model input.

Therefore, we follow a different approach and build a verification method on top of the respiratory model to deduce data that actually *can* be verified. This verification method is based on the clinically used monitoring method of electrical impedance tomography (EIT) [70]. EIT is a non-invasive, radiation-free imaging modality with low spatial and high temporal resolution that allows the assessment of regional ventilation distribution at bedside. In commercially available EIT systems a set of electrodes is placed on the patient's chest circumference in one plane. To generate EIT images, small alternating currents are generated at high frequency, usually between adjacent pairs of electrodes. The resulting potential differences are detected by the remaining set of electrodes. By rotating the current injection pair around the chest circumference, a set of $N = 208$ voltage measurements is obtained if 16 electrodes are used. This data is subsequently used for image reconstruction using a difference reconstruction algorithm such as the Graz consensus reconstruction algorithm for EIT (GREIT) [71]. The resulting image visualises dynamic regional changes in electrical bioimpedance of lung tissue and thus the amount of regionally contained insulating air against a predefined baseline, usually the fully expired state. If more air is contained in the alveoli, tissue bioimpedance will increase locally, resulting in higher voltage measurements for the corresponding region.

A detailed description of the coupling of respiratory models with EIT can be found elsewhere [67] and we will limit to the main ideas here visualised in Fig. 7. Regional ventilation comes from any of the previously described models. This ventilation can be transferred towards a local tissue conductivity using experimental or computational data [72–74]. This conductivity data are mapped to a real thorax model of the current patient. EIT electrodes are positioned in the model where they are placed on the real patient and virtual EIT monitoring is performed computationally applying the same stimulating currents to the patient as is done in reality. Voltages can then be computed solving the Laplace equation and be compared to clinically measured voltages for the same stimulation patterns. Further, similar image reconstruction algorithms [71] can be used to reconstruct a regional distribution of conductivities in the imaged plane at a temporal resolution of 50 Hz. This allows a highly dynamic and regional validation of computed and measured regional ventilation for any ventilation protocol.

As EIT imaging is not used for generation of the respiratory model, this can be seen as rigorous and clinically realisable validation method for the next generation of personalised coupled respiratory models. With virtual EIT being a computational replication of clinical EIT measurements, it is important to consider potential limitations of the EIT principle also for model validation. One major factor in this context is the low spatial resolution of

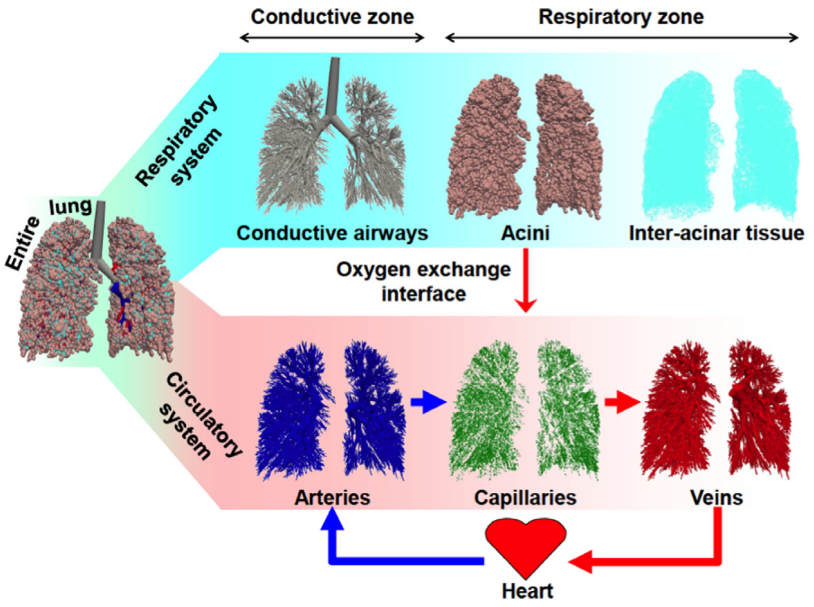

Fig. 8. Coupling of models of the respiratory and circulatory system. The entire lung model consists of the respiratory (top row) and the circulatory system (bottom row). The respiratory system includes the conducting airways, pulmonary acini and the inter-acinar tissue presented in Section 2. The circulatory system consists of arteries, capillaries and veins which are connected via the heart. Oxygen exchange takes place between the acini and the capillaries via diffusion across a defined interface for each acinus (see Section 3.2.2).

EIT, which means that the computational lung model usually delivers results at higher resolution (depending on the resolution of the CT data used for model generation, usually approximately 2.0 mm) than reconstructed EIT images (resolution approximately 2.0 cm). Consequently, rigorous validation can only be ensured on the spatial resolution of the EIT. For validation of e.g., computed dynamic heterogeneity during ventilation, the spatial resolution of EIT in combination with its high temporal resolution is, however, well suited [75]. A further important aspect is that changes in regional conductivity are not only a consequence of air content, but also of the distribution of electrically conductive blood flowing through the pulmonary arteries, capillaries and veins. Therefore, more accurate validation with clinically measured EIT would require the pulmonary circulation to be modelled as presented in Section 3.2.

In conclusion, we believe that virtual EIT offers a fast and easy realisable validation method for many kinds of personalised respiratory models. It is the first approach that allows validation of computed regional strains in the lung—a quantity which has recently been directly linked to the onset and progression of respiratory diseases [55]. Further, EIT is currently the only known method applicable in the intensive care unit without doing any harm to the patient. The fact that no additional fitting is required for the virtual EIT, the possibility for continuous verification in real time with the computation of ventilation, and the availability of the virtual EIT images in a clinically familiar format hopefully generate further trust in computational lung modelling. On the computational modelling side, a detailed validation of the developed models offers a chance for identifying and improving potential limitations of the proposed coupled approaches if required.

3.2. Towards a reduced-dimensional entire lung model including gas exchange

Up to now several realistic models have been presented to investigate ventilation under various conditions. However, while being able to get a lot of important information like for example regional ventilation and tissue strains, so far it is not clear, if optimised regional ventilation leads to expected and desired gas transport and exchange between air and blood. Therefore, in this section, a one-dimensional model of the pulmonary circulatory system is derived and connected to the *0D/0D* respiratory model. The resulting entire lung model (Fig. 8) enables a coupled simulation of airflow, tissue inflation, and perfusion which can be used e.g., to evaluate the suitability of different ventilation protocols with regard to sufficient blood oxygenation.

3.2.1. Geometry generation

In the human lung, the vasculature is situated in close vicinity of the airway tree. Pulmonary arteries branch and lie parallel to the airways, whereas pulmonary veins lie between the airways and the pulmonary arteries [58]. Based on this anatomical knowledge, pulmonary blood vessels are generated from the reduced-dimensional airway tree.

At each branching node of the airway tree, a translation vector $\boldsymbol{a}$ is computed to shift the nodes of the associated arterial tree, i.e.,

$$\boldsymbol{a} = (r_{\text{art}} + r_{\text{aw}}) \frac{\boldsymbol{u}_{\text{d1}} \times \boldsymbol{u}_{\text{d2}}}{||\boldsymbol{u}_{\text{d1}} \times \boldsymbol{u}_{\text{d2}}||_2} \tag{1}$$

with $\boldsymbol{u}_{\text{d1}}, \boldsymbol{u}_{\text{d2}}$ denoting the orientation vectors of the daughter branches d1, d2 and $r_{\text{art}}, r_{\text{aw}}$ being the radii of the artery and associated airway. The radius of each artery is given by

$$\tilde{r}_{\text{art}} = \hat{r}_{\text{art;G}} * f = r_{\text{art;0}}\, 2^{-\text{G}/3} * \frac{r_{\text{aw}}}{\hat{r}_{\text{aw;G}}} \tag{2}$$

where $r_{\text{art;0}}$ refers to the radius of a pulmonary artery at generation zero and $\hat{r}_{\text{art;G}}$ is the average radius of an artery in generation G according to [58]. To maintain the natural asymmetry in the arterial tree, $\hat{r}_{\text{art;G}}$ is multiplied by the ratio f of the artery's corresponding airway radius r_{aw} to the mean airway radius of this particular generation $\hat{r}_{\text{aw;G}}$. After calculation of the volume of the generated arterial tree $\tilde{V}_{\text{art}}$, the arterial radius is corrected by a factor $\alpha_{\text{art}} = V_{\text{art}}/\tilde{V}_{\text{art}}$ to match the patient's actual arterial volume V_{art}, i.e., $r_{\text{art}} = \tilde{r}_{\text{art}} * \alpha_{\text{art}}$.

To create a geometry of the pulmonary veins, each branching point b of the airway tree is first shifted to the midpoint of the associated daughter nodes. Hence, the following translation vector is applied

$$\boldsymbol{v}_1 = (\boldsymbol{x}_{\text{d1}} + \boldsymbol{x}_{\text{d2}})/2 - \boldsymbol{x}_{\text{b}} \tag{3}$$

with $\boldsymbol{x}_{\text{b}}, \boldsymbol{x}_{\text{d1}}, \boldsymbol{x}_{\text{d2}}$ denoting the location vectors of the branching and daughter nodes, respectively. Subsequently, the modified tree is translated analogously to the arterial tree using the nodal translation vector $\boldsymbol{v}_2$ given by

$$\boldsymbol{v}_2 = -(r_{\text{ven}} + r_{\text{aw}}) \frac{\boldsymbol{u}_{d1} \times \boldsymbol{u}_{d2}}{||\boldsymbol{u}_{d1} \times \boldsymbol{u}_{d2}||_2} \tag{4}$$

where the minus sign indicates an inversion of the translation vector compared to (1) and r_{ven} is the venous radius

$$\tilde{r}_{\text{ven}} = \hat{r}_{\text{ven;G}} * f = r_{\text{ven;0}}\, 2^{-\text{G}/3} * \frac{r_{\text{aw}}}{\hat{r}_{\text{aw;G}}}. \tag{5}$$

Again, the natural asymmetry in the venous tree is accounted for by multiplying the average venous radius $\hat{r}_{\text{ven;G}}$ by f. After calculation of the volume of the generated venous tree $\tilde{V}_{\text{ven}}$, the venous radius is also corrected by a factor $\alpha_{\text{ven}} = V_{\text{ven}}/\tilde{V}_{\text{ven}}$ to match the patient's actual venous volume V_{ven}, i.e., $r_{\text{ven}} = \tilde{r}_{\text{ven}} * \alpha_{\text{ven}}$.

Between each terminal artery and vein, a network of capillaries is grown in an iterative manner based on the following assumptions: (i) the network consists of two connected, symmetric trees; (ii) each tree is bifurcating [76]; (iii) the fixed length to radius ratios are $\text{lr}_{\text{artl}} = 12$ for arterioles and $\text{lr}_{\text{venl}} = 14$ for venules [77]; (iv) the venules radius to arterioles radius ratio r_{va} is 1.44 [77]; (v) the terminating blood capillary radius r_{term} is 4 μm [78]; (vi) the daughter to parent radius relationship α_{dp} is $0.5^{1/3}$ following Murray's law [79] for laminar flow.

The total volume V_{artl} of arterioles in a tree of N generations then reads

$$V_{\text{artl}} = V_{\text{artl;0}} \sum_{n=0}^{N} (\alpha_{\text{dp}})^{3n} 2^n = \pi (r_{\text{artl;0}})^3\, \text{lr}_{\text{artl}} \sum_{n=0}^{N} (\alpha_{\text{dp}})^{3n} 2^n \tag{6}$$

where $r_{\text{artl;0}}$ and $V_{\text{artl;0}}$ refer to the radius and the volume of the root arteriole in the tree of capillaries, respectively. Similarly, the total volume V_{venl} of venules in a tree of n generations is given by

$$V_{\text{venl}} = \pi (r_{\text{venl;0}})^3\, \text{lr}_{\text{venl}} \sum_{n=0}^{N} (\alpha_{\text{dp}})^{3n} 2^n = \pi \left(r_{\text{artl;0}}\, r_{\text{va}}\right)^3\, \text{lr}_{\text{venl}} \sum_{n=0}^{N} (\alpha_{\text{dp}})^{3n} 2^n. \tag{7}$$

Hence, the overall volume of the capillary network connecting a terminal artery and vein can be calculated as follows

$$V_{\text{cap}} = \pi (r_{\text{artl};0})^3 \left(\text{lr}_{\text{artl}} + (r_{\text{va}})^3 \text{lr}_{\text{venl}} \right) \sum_{n=0}^{N} (\alpha_{\text{dp}})^{3n} 2^n. \tag{8}$$

At the same time, V_{cap} is given by

$$V_{\text{cap}} = V_{\text{cap;tot}} \frac{V_{\text{ac}}}{V_{\text{ac;tot}}} \tag{9}$$

where $V_{\text{cap;tot}}$, V_{ac}, $V_{\text{ac;tot}}$ denote the patient's overall capillary blood volume, the volume of the associated acinar tree, and the total volume of air in the respiratory zone. From (8) and (9), the number N of generations minimising $||r_{\text{artl};0} (\alpha_{\text{dp}})^N - r_{\text{term}}||_2$ is determined iteratively.

For our patient taken from [9] the total volumes of blood in pulmonary arteries, veins, and capillaries are set to $V_{\text{art;tot}} = 135$ ml, $V_{\text{ven;tot}} = 235$ ml, and $V_{\text{cap;tot}} = 80$ ml, respectively [80]. Using this data, pulmonary circulation models created based on the procedure described above show a very good agreement with reported morphological measurements [58].

3.2.2. Mathematical model

For simulating blood flow in the pulmonary circulatory system, the same set of governing equations as for 1D deformable pipe flow is used [50,51].

The transport and exchange of oxygen is formulated in terms of the concentration of oxygen in a fluid defined by

$$c_s = \frac{n_{\text{O}_2}}{V_{\text{f}}} \tag{10}$$

where n_{O_2} is the number of moles of oxygen and V_{f} the volume of fluid (i.e., air or blood) in which O_2 is dissolved. In pulmonary mechanics, oxygen concentration is measured by the O_2 partial pressure which is, however, defined differently in air and blood. The oxygen partial pressure in air $P_{\text{O}_2;\text{air}}$ is the amount of pressure O_2 contributes to the atmospheric pressure, reading

$$c_s = \frac{P_{\text{O}_2;\text{air}}}{RT} \tag{11}$$

with R denoting the gas constant and T being the temperature in degrees Kelvin. The oxygen partial pressure in blood $P_{\text{O}_2;\text{bld}}$ is defined via a saturation curve [81] as the volume of oxygen that is absorbed by haemoglobin when exposed to air with a certain oxygen partial pressure, i.e.,

$$c_s = \frac{V_{\text{O}_2;\text{sat}}}{V_{\text{m}} V_{\text{bld}}} \left(\frac{(P_{\text{O}_2;\text{bld}})^{\xi}}{(P_{\text{O}_2;\text{bld}})^{\xi} + (\tilde{P}_{\text{O}_2})^{\xi}} \right) \tag{12}$$

where $\xi = 2.5$. $V_{\text{O}_2;\text{sat}}$ denotes the 100% saturation volume of oxygen in blood, $V_{\text{m}} = 22.4$ l/mol refers to the molar volume of any gas at standard temperature and pressure, V_{bld} is the volume of blood, and $\tilde{P}_{\text{O}_2}$ is the oxygen partial pressure at 50% oxygen saturation.

To formulate the one-dimensional transport equation of oxygen, it is assumed that O_2 (i) is mixed fully within a cross-sectional area and (ii) is neither deposited nor generated except at the O_2 exchange interface. The balance of O_2 molecules in an infinitesimal 1D pipe element (with length $\text{d}x$, volume V, and cross-sectional area A) then reads

$$\frac{\partial (c_s V)}{\partial t} = J\left(x - \frac{\text{d}x}{2}\right) - J\left(x + \frac{\text{d}x}{2}\right) \tag{13}$$

with

$$J(x) = Q c_s(x) - D_{\text{O}_2} A \frac{\partial c_s(x)}{\partial x} \tag{14}$$

being the O_2 flux including convective and diffusive transport. Q is the flow rate of the fluid carrying O_2 and D_{O_2} refers to the O_2 diffusion coefficient. If the right-hand side of (13) is replaced by a first-order Taylor series approximation

and higher-order terms are neglected, (13) becomes

$$V\frac{\partial c_s}{\partial t}+c_s\frac{\partial V}{\partial t}=-Q\frac{\partial c_s}{\partial x}\mathrm{d}x-c_s\frac{\partial Q}{\partial x}\mathrm{d}x+D_{\mathrm{O}_2}A\frac{\partial^2 c_s}{\partial x^2}\mathrm{d}x+D_{\mathrm{O}_2}\frac{\partial A}{\partial x}\frac{\partial c_s}{\partial x}\mathrm{d}x. \tag{15}$$

Introducing the plain strain assumption and the mass conservation of the fluid carrying O_2, i.e.,

$$\frac{\partial Q}{\partial x}=-\frac{\partial A}{\partial t}, \tag{16}$$

the equation finally describing O_2 transport is given by

$$\frac{\partial c_s}{\partial t}+\frac{Q}{A}\frac{\partial c_s}{\partial x}=D_{\mathrm{O}_2}\frac{\partial^2 c_s}{\partial x^2}+D_{\mathrm{O}_2}\frac{1}{A}\frac{\partial A}{\partial x}\frac{\partial c_s}{\partial x}. \tag{17}$$

Eq. (17) is solved explicitly in time using an upwind forward Euler scheme. Hence, the concentration of oxygen is only prescribed at an inflow boundary. At a junction, it is assumed that O_2 fully mixes and the volume of the junction is negligible. Consequently, all daughter vessels have the same concentration of O_2, which in case of a bifurcating tree equals the concentration of O_2 in the parent vessel.

With (17), the transport of air can be described in both the airway tree and the pulmonary circulatory system. The exchange of O_2 between air and blood happens at the acinar level. In this work, each terminal airway is associated with one terminal artery and one terminal vein. Hence, each capillary network can be assigned to one acinus. To model the diffusion of oxygen from a high O_2 concentration medium (i.e., the air in the acinus) to a low O_2 concentration medium (i.e., the capillary blood), Fick's law is used [82,83]. Hence, the volumetric flow rate Q_{O_2} of the O_2 molecules at the interface reads

$$Q_{\mathrm{O}_2}=D^{\mathrm{I}}\left(P_{\mathrm{O}_2;\mathrm{air}}-P_{\mathrm{O}_2;\mathrm{bld}}\right). \tag{18}$$

The interface diffusion constant D^{I} is given by

$$D^{\mathrm{I}}=D^{\mathrm{I}}_{\mathrm{O}_2}\frac{A^{\mathrm{I}}_{\mathrm{O}_2}}{h^{\mathrm{I}}_{\mathrm{O}_2}} \tag{19}$$

where $D^{\mathrm{I}}_{\mathrm{O}_2}$ is an O_2 diffusion constant, $h^{\mathrm{I}}_{\mathrm{O}_2}$ is the O_2 interface thickness, and $A^{\mathrm{I}}_{\mathrm{O}_2}$ is the total common surface between the alveoli and the blood capillaries. In [84], the overall alveolar surface area A_{ac} of an acinus with volume V_{ac} which is composed of N_{ad} alveolar ducts based on the model of Denny and Schroter [39] has been derived. Knowing that 90% of the alveolar surface is in contact with blood capillaries [85], $A^{\mathrm{I}}_{\mathrm{O}_2}$ is obtained as

$$A^{\mathrm{I}}_{\mathrm{O}_2}=0.9A_{\mathrm{ac}}=0.9N_{\mathrm{ad}}\left(168+345\sqrt{3}\right)\left(\frac{V_{\mathrm{ac}}}{288N_{\mathrm{ad}}\sqrt{2}}\right)^{2/3}. \tag{20}$$

3.2.3. Parameter identification

Capillaries are known to make up most of the resistance and least of the compliance of the pulmonary circulatory system [86]. Consequently, each capillary network can be assumed as a stiff resistive tree with an overall resistance given by Poiseuille's law

$$R_{\mathrm{cap}}=\sum_{n=0}^{N_{\mathrm{res}}}\left(\frac{8\mu_{\mathrm{bld}}L_{\mathrm{artl};0}}{2^n\pi(\alpha_{\mathrm{dp}})^{3n}(r_{\mathrm{artl};0})^4}\right)+\sum_{n=0}^{N_{\mathrm{res}}}\left(\frac{8\mu_{\mathrm{bld}}L_{\mathrm{venl};0}}{2^n\pi(\alpha_{\mathrm{dp}})^{3n}(r_{\mathrm{venl};0})^4}\right) \tag{21}$$

where μ_{bld}, $L_{\mathrm{artl};0}$, and $L_{\mathrm{venl};0}$ denote the blood viscosity, the initial arteriole and venule length, respectively. Due to the large number of bifurcations, the effects of the very small blood vessels disappear [57]. Following [76], only the contributions of capillary generations with radius greater or equal to $r_{\mathrm{res}}=0.15$ mm are taken into account in (21). Hence, the number of considered capillary generations N_{res} can be determined from $r_{\mathrm{res}}=(\alpha_{\mathrm{dp}})^{N_{\mathrm{res}}}r_{\mathrm{artl};0}$.

In healthy adult humans, the arterial stiffness E_{art} is four times higher than the venous stiffness E_{ven} [85]. Apart from this information, however, little is known about the material properties of the pulmonary blood vessels. Assuming

constant arterial and venous stiffness in the pulmonary circulatory system, E_{art} can be found iteratively by solving the following problem

$$\begin{aligned} &\underset{f_P}{\text{minimise}} \quad f_P = |P_{\text{PV;max}} - P_{\text{systolic}}| + |P_{\text{PV;min}} - P_{\text{diastolic}}| \\ &\text{subject to} \quad Q_{\text{PV}}(t) = \begin{cases} Q_{\max}\left[1+\cos(2\pi t/T_{\text{sys}})\right] & 0 \le t_{\text{cyc}} \le T_{\text{sys}} \\ 0 & T_{\text{sys}} < t_{\text{cyc}} < T_{\text{dia}} \end{cases}, \\ &\qquad\quad E_{\text{ven}} = \frac{E_{\text{art}}}{4} \end{aligned} \tag{22}$$

where Q_{PV} is the blood flow rate at the pulmonary valve, $Q_{\max}$ is the peak pulmonary valve flow rate, $t_{\text{cyc}} = t - n_{\text{cyc}}T$, n_{cyc} is the cardiac cycle number, $T = 1$ s is the period of a cardiac cycle, and $T_{\text{sys}} = 0.3$ s is the period of the systolic phase. $P_{\text{PV;max}}$ and $P_{\text{PV;min}}$ denote the peak and minimum pulmonary valve blood pressure, whereas $P_{\text{systolic}} = 23$ mmHg and $P_{\text{diastolic}} = 4$ mmHg are the systolic and diastolic blood pressure, respectively. The cardiac output is taken to be $\frac{1}{T}\int_0^T Q_{\text{PV}}\mathrm{d}t = 5$ l/min and the blood pressure at the atrium side is prescribed as 0 mmHg. The viscous constant of the blood vessel wall γ_s is given by

$$\gamma_s = \frac{T_s \tan(\phi_s)}{4\pi}\beta_s = \frac{T_s \tan(\phi_s)}{4\pi}\sqrt{\pi}\frac{h_s E_s}{1-\nu_s^2} \tag{23}$$

with ν_s denoting the wall Poisson ratio, E_s referring to the wall Young's modulus, $\phi_s = 11°$, and $T_s = T_{\text{sys}}$ [87]. The wall thickness h_s can be found using the empirical model described in [76]. Solution of the optimisation problem resulted in an arterial stiffness of $E_{\text{art}} = 250$ kPa which successfully reproduced the systolic and diastolic blood pressures. The mean pulmonary pressure fell within the measurable data of [88].

All parameters associated with oxygen transport and exchange can be taken from literature. The oxygen partial pressure in blood at 50% oxygen saturation is $\tilde{P}_{\text{O}_2} = 26$ mmHg [81] and the 100% saturation volume of oxygen in blood is $V_{\text{O}_2;\text{sat}} = 0.208 V_{\text{bld}}$ [83]. The oxygen diffusion coefficients in air and blood are found to be $D_{\text{O}_2;\text{air}} = 22.34$ mm^2 s^{-1} [89] and $D_{\text{O}_2;\text{bld}} = 2 \cdot 10^{-3}$ mm^2 s^{-1} [90], respectively. Furthermore, the diffusion coefficient of the alveolar interface separating air from blood is found to be $D^{\text{I}}_{\text{O}_2} = 3 \cdot 10^{-9}$ mm^2 s^{-1} mmHg^{-1} [83]. In [84], the O_2 transport model parameters defined above were shown to reproduce physiologically reasonable results in simple numerical experiments.

3.2.4. Numerical example

To illustrate the capability of the presented entire lung model, the distribution of P_{O_2} is studied in a patient-specific lung model for which the ventilatory part is in detail presented in [9]. Mechanical ventilation of a 42 year old patient (functional residual capacity $V_{FRC} = 2.65$l, total lung capacity $V_{TLC} = 4.76$l) is simulated for supine position and volume controlled mechanical ventilation. The ventilator is modelled as

$$\begin{cases} Q_t = 500/T_{\text{q}}\text{ml} & (N_{\text{cyc}}-1)T \le t < (N_{\text{cyc}}-1)T + T_{\text{q}} \\ Q_t = 0\text{ ml} & (N_{\text{cyc}}-1)T + T_{\text{q}} \le t < (N_{\text{cyc}}-1)T + T_{\text{q}} + T_0 \\ P_t = 0\text{ cmH}_2\text{O} & (N_{\text{cyc}}-1)T + T_{\text{q}} + T_0 \le t < N_{\text{cyc}}T \end{cases} \tag{24}$$

where $T = 4$ s is the total period of a mechanical ventilation cycle, N_{cyc} is the ventilation cycle number, $T_{\text{q}} = 1.5$ s is the period of time in which air is enforced into the lung, $T_0 = 0.25$ s is the period of time in which air is trapped inside the lung, Q_t is the tracheal flow rate, and P_t is the tracheal pressure. Pleural pressure is obtained from a literature-based thorax boundary condition [91] and gravity is accounted for in supine positioning.

A fixed heart rate of 60 beats per minute and a cardiac output of 5 l/min are prescribed at the pulmonary ventricle. The circulatory system is subjected to an external pressure equivalent to pleural pressure and to the blood's gravitational pressure

$$P_{\text{bld;g}} = \rho_{\text{bld}}\langle \boldsymbol{x} - \boldsymbol{x}_0,\, g\,\boldsymbol{n}_{\text{g}}\rangle \tag{25}$$

where ρ_{bld} is the density of blood, $\boldsymbol{x}$ is the spatial coordinate of any point in the lung, $\boldsymbol{x}_0$ is a reference point defined as centerpoint in gravitational direction $\boldsymbol{n}_g$, and g is the acceleration due to gravity. At the terminals of the pulmonary veins, the atrium is supposed to have a zero pressure.

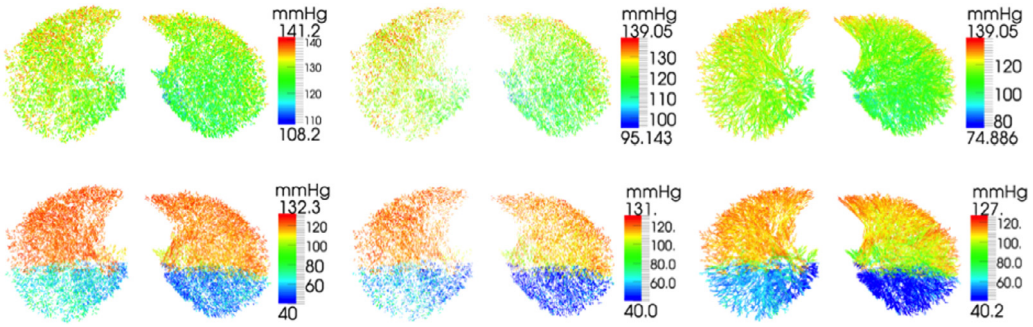

Fig. 9. Distribution of P_{O_2} in the respiratory zone (left), blood capillaries (middle), and pulmonary veins (right) of the healthy (top) and diseased (bottom) mechanically ventilated lung in supine position.

The distribution of oxygen is simulated in both a healthy lung and a simple model of a diseased lung. In the latter case, all peripheral conducting airways within a region of 5 cm away from the back are occluded. In both cases, a time step of $\Delta t = 1$ ms is used and a periodic steady-state is computed.

The spatial distribution of P_{O_2} in the mechanically ventilated healthy and modelled diseased lung are shown in Fig. 9. It can be clearly observed that in the diseased lung only the blood within the healthy (i.e., recruited) section is oxygenated. Consequently, the average blood P_{O_2} returned back to the heart drops from 111 mmHg for the healthy lung to only 70 mmHg for the diseased lung.

3.2.5. Discussion

Computation of the spatial distribution of oxygen partial pressure P_{O_2} provides an important insight as it shows for the first time the effect of deteriorated ventilation on oxygenation and perfusion locally. For investigations in respiratory mechanics, such an approach opens up new possibilities. First, processes in oxygenation and CO_2 clearance e.g., during high-frequency ventilation [92] which are not fully understood today, can be simulated. Further, patient-specific ventilatory treatment can be improved by guiding ventilation in a way such that not only ventilation but also perfusion is maximised. In our simulated derecruited patient example, this would potentially lead to more pronounced ventilation in the ventral region, however, also the perfusion during and after a recruitment manoeuvre would be extremely interesting.

Compared to previous approaches of oxygen transport [4,93] our approach is computed on a realistic patient-specific representation of both airways and blood vessels with perfect match of anatomical data [57,58]. For further extension of the gas exchange model, several directions are proposed in the following: First, the assumption of homogeneous distribution of oxygen within an airway/vessel cross-section might be limited for certain respiratory patterns such as the previously mentioned high-frequency ventilation [92] and needs further investigation. Also, in many cases, respiratory dysfunction comes along with changes in shape or thickness of the blood-gas barrier in the alveolar wall and thus can significantly slow down diffusion processes. In such cases, regionally varying diffusion constants would be necessary to adequately model compromised gas exchange and to correctly estimate the transferred amount of oxygen.

Still, the proposed model of oxygen transport outlines the primary function of the lung: gas exchange. This exchange process is not only governed by regional ventilation but also by the heterogenity of perfusion due to body posture or a patient's anatomy of the blood vessels. An important message from this section is that, in reality, optimising ventilation is far more complex than improving pure respiratory quantities. Finally, the pulmonary circulation and the gas exchange with the respiratory system have to be included in future entire lung models addressing the challenge of optimised personalised ventilation.

4. Conclusion

The main conclusion of this article is that realistic respiratory models based on the underlying physics of airflow dynamics and tissue properties is more powerful than existing clinical/physiological black-box parametrisations of global lung behaviour based on functional measurements. Accurate mathematical descriptions of the lung, however,

require to model the coupling between airflow and lung tissue to fully include all essential features of the respiratory system.

Different clinical and scientific questions and the variety of physical fields and scales of the respiratory system and their interaction consequently call for the application of different models at different levels of complexity tailored to the current problem under investigation. Sophisticated and computationally extremely expensive fully resolved models should only be applied where inevitable for an insight into single details and simpler approaches can be integrated for other effects to ensure an optimal use of the available computational resources in answering the current problem. Simulations of transitional and turbulent flow phenomena in the upper airways e.g., require fully resolved three-dimensional models, whereas purely quantification of pressure and flow distributions in the higher tree generations can be modelled using the concept of dimensional reduction. This clearly shows that there is no "one-size-fits-all" approach in respiratory mechanics, but rather a need for a toolbox of modern methods in computational biomechanics which can be combined and adopted to suit problem-specific needs.

Once validated with classical lung function measurements on a global, and electrical impedance tomography (EIT) images on a highly dynamic and local scale, an appropriate computational lung model can present its predictive character to (i) study isolated effects which are hard or not at all to assess in a subject *in vivo*, (ii) to advance medical imaging and functional diagnostics by incorporating computational models that are based on the underlying physics, and (iii) to finally assist in patient-specific treatment planning and optimisation.

One ultimate goal in respiratory modelling must be the simulation of gas exchange and lung perfusion as soon as ventilation is sufficiently understood. In this article, we made further steps towards this goal with the first realisation of gas exchange on a patient-specific pulmonary circulatory tree giving a direction for potential future research in this particular field of computational biomechanics.

References

[1] K.G. Hickling, The pressure-volume curve is greatly modified by recruitment – A mathematical model of ARDS lungs, Am. J. Respir. Crit. Care Med. 158 (1998) 194–202.

[2] J.G. Venegas, R.S. Harris, B.A. Simon, A comprehensive equation for the pulmonary pressure-volume curve, J. Appl. Physiol. 84 (1998) 389–395.

[3] J.H.T. Bates, Lung Mechanics – An Inverse Modeling Approach, Cambridge University Press, 2009.

[4] B. Maury, The Respiratory System in Equations, Modeling, Simulation and Applications, Vol. 7, Springer-Verlag, Italia, 2013.

[5] K.S. Burrowes, P.J. Hunter, M.H. Tawhai, Anatomically based finite element models of the human pulmonary arterial and venous trees including supernumerary vessels, J. Appl. Physiol. 99 (2005) 731–738.

[6] M.H. Tawhai, J.H.T. Bates, Multi-scale lung modeling, J. Appl. Physiol. 110 (2011) 1466–1472.

[7] M. Ismail, A. Comerford, W.A. Wall, Coupled and reduced dimensional modeling of respiratory mechanics during spontaneous breathing, Int. J. Numer. Methods Biomed. Eng. 29 (2013) 1285–1305.

[8] L.U. Berger, R. Bordas, K. Burrowes, C.E. Brightling, R. Hartley, D. Kay, Understanding the interdependence between parenchymal deformation and ventilation in obstructive lung disease, in: Dynamics of Airway Narrowing in Asthma: Still Misunderstood? vol. B30, American Thoracic Society, 2014.

[9] C.J. Roth, M. Ismail, L. Yoshihara, W.A. Wall, A comprehensive computational human lung model incorporating interacinar dependencies: Application to spontaneous breathing and mechanical ventilation, Int. J. Numer. Meth. Biomed. Engng. (2016) in press.

[10] J.B. Grotberg, Respiratory fluid mechanics and transport processes, Annu. Rev. Biomed. Eng. 3 (2001) 421–457.

[11] J.B. Grotberg, Respiratory fluid mechanics, Phys. Fluids 23 (2011) 021301.

[12] C.D. Bertram, D.P. Gaver, Biofluid mechanics of the pulmonary system, Ann. Biomed. Eng. 33 (2005) 1681–1688.

[13] B. Ma, K.R. Lutchen, An anatomically based hybrid computational model of the human lung and its application to low frequency oscillatory mechanics, Ann. Biomed. Eng. 14 (2006) 1691–1704.

[14] C.-L. Lin, M.H. Tawhai, G. McLennan, E.A. Hoffman, Characteristics of the turbulent laryngeal jet and its effect on airflow in the human intra-thoracic airways, Respir. Physiol. Neurobiol. 157 (2007) 295–309.

[15] A. Comerford, G. Bauer, W.A. Wall, Nanoparticle transport in a realistic model of the tracheobronchial region, Int. J. Numer. Meth. Biomed. Engng. 26 (2010) 904–914.

[16] A. Comerford, C. Förster, W.A. Wall, Structured tree impedance outflow boundary conditions for 3d lung simulations, J. Biomech. Eng. 132 (2010) 10 pages.

[17] A. Comerford, V. Gravemeier, W.A. Wall, An algebraic variational multiscale-multigrid method for large-eddy simulation of turbulent pulsatile flows in complex geometries with detailed insight into pulmonary airway flow, Internat. J. Numer. Methods Fluids 71 (2013) 1207–1225.

[18] Y. Yin, J. Choi, E.A. Hoffman, M.H. Tawhai, C.-L. Lin, A multiscale mdct image-based breathing lung model with timevarying regional ventilation, J. Comput. Phys. 244 (2013) 168–192.

[19] K.S. Burrowes, R.B. Buxton, G.K. Prisk, Assessing potential errors of mri-based measurements of pulmonary blood flow using a detailed network flow model, J. Appl. Physiol. 113 (2012) 130–141.

[20] Y. Yin, J. Choi, A.H. Hoffman, M.H. Tawhai, C.-L. Lin, Simulation of pulmonary airflow with a subject-specific boundary condition, J. Biomech. 43 (2010) 2159–2163.
[21] Y. Yin, J. Choi, E.A. Hoffman, M.H. Tawhai, C.-L. Lin, A multiscale mdct image-based breathing lung model with time-varying regional ventilation, J. Comput. Phys. 244 (2013) 168–192.
[22] Z. Zhang, C. Kleinstreuer, Airflow structures and nano-particle deposition in a human upper airway model, J. Comput. Phys. 198 (2004) 178–210.
[23] B. Ma, K. Lutchen, CFD simulation of aerosol deposition in an anatomically based human large–medium airway model, Ann. Biomed. Eng. 37 (2009) 271–285.
[24] C. Kleinstreuer, Z. Zhang, Airflow and particle transport in the human respiratory system, Annu. Rev. Fluid Mech. 42 (2010) 301–334.
[25] S.N. Ghadiali, D.P. Gaver, Biomechanics of liquid-epithelium interactions in pulmonary airways, Respir. Physiol. Neurobiol. 163 (2008) 232–243.
[26] A.L. Hazel, M. Heil, Finite-Reynolds-number effects in steady, three-dimensional airway reopening, J. Biomech. Eng. 128 (2005) 573–578.
[27] W.A. Wall, T. Rabczuk, Fluid–structure interaction in lower airways of ct-based lung geometries, Internat. J. Numer. Methods Fluids 57 (2008) 653–675.
[28] G. Xia, M.H. Tawhai, E.A. Hoffman, C.-L. Lin, Airway wall stiffening increases peak wall shear stress: A fluid–structure interaction study in rigid and compliant airways, Ann. Biomed. Eng. 38 (2010) 1836–1853.
[29] L. Yoshihara, C.J. Roth, W.A. Wall, Fluid–structure interaction including volumetric coupling with homogenised subdomains for modeling respiratory mechanics, Int. J. Numer. Meth. Biomed. Engng. (2016) in press.
[30] S.M.K. Rausch, D. Haberthur, M. Stampanoni, J.C. Schittny, W.A. Wall, Local strain distribution in real threedimensional alveolar geometries, Ann. Biomed. Eng. 39 (2011) 2835–2843.
[31] H. Oertel jr., Prandtl - Essentials of Fluid Mechanics, third ed., Springer, 2010.
[32] F. Verdugo, C.J. Roth, L. Yoshihara, W.A. Wall, Efficient solvers for coupled models in respiratory mechanics, Int. J. Numer. Meth. Biomed. Engng. (2016) in press.
[33] V. Gravemeier, A. Comerford, L. Yoshihara, M. Ismail, W.A. Wall, A novel formulation for Neumann inflow boundary conditions in biomechanics, Int. J. Numer. Meth. Biomed. Engng. 28 (2012) 560–573.
[34] C. Bertoglio, A. Caiazzo, A tangential regularization method for backflow stabilization in hemodynamics, J. Comput. Phys. 261 (2014) 162–171.
[35] L. Wiechert, W.A. Wall, A nested dynamic multi-scale approach for 3d problems accounting for micro-scale multi-physics, Comput. Methods. Appl. Math. 199 (2010) 1342–1351.
[36] A. Slutsky, Ventilator-induced lung injury, N. Engl. J. Med. 369 (2013) 2126–2136.
[37] N. Jahani, X.S. Choi, J. Choi, K. Iyer, E.A. Hoffman, C.-L. Lin, Assessment of regional ventilation and deformation using 4D-CT imaging for healthy human lungs during tidal breathing, J. Appl. Physiol. 119 (2015) 1064–1074.
[38] E. Denny, R. Schroter, The mechanical behavior of mammalian lung alveolar duct model, J. Biomech. Eng. 117 (1995) 254–261.
[39] E. Denny, R. Schroter, Relationships between alveolar size and fiber distribution in a mammalian lung alveolar duct model, J. Biomech. Eng. 119 (1997) 289–297.
[40] E. Denny, R.C. Schroter, Viscoelastic behavior of a lung alveolar duct model, J. Biomech. Eng. 122 (2000) 143–151.
[41] S.R. Khangure, P.B. Noble, A. Sharma, P.Y. Chia, P.K. McFawn, H.W. Mitchell, Cyclical elongation regulates contractile responses of isolated airways, J. Appl. Physiol. 97 (2004) 913–919.
[42] J.M. Oakes, A.L. Marsden, C. Grandmont, S.C. Shadden, C. Darquenne, I.E. Vignon-Clementel, Airflow and particle deposition simulations in health and emphysema: From in vivo to in silico animal experiments, Ann. Biomed. Eng 42 (2014) 899–914.
[43] L. Boudin, C. Grandmont, A. Lorz, A. Moussa, Modelling and numerics for respiratory aerosols, Commun. Comput. Phys. 18 (2015) 723–756.
[44] C. Grandmont, B. Maury, A. Soualah, Multiscale modelling of the respiratory track: a theoretical framework, ESAIM Proc. 23 (2008) 10–29.
[45] J. Choi, G. Xia, M.H. Tawhai, E.A. Hoffman, C.L. Lin, Numerical study of high-frequency oscillatory air flow and convective mixing in a CT-based human airway model, Ann. Biomed. Eng. 38 (2010) 3550–3571.
[46] A.J. Bates, D.J. Doorly, R. Cetto, H. Calmet, A.M. Gambaruto, N.S. Tolley, G. Houzeaux, R.C. Schroter, Dynamics of airflow in a short inhalation, J. R. Soc. Interface 12 (2014) 20140880.
[47] A.J. Bates, A. Comerford, R. Cetto, R.C. Schroter, N.S. Tolley, D.J. Doorly, Power loss mechanisms in pathological tracheas, J. Biomech. S0021-9290 (2015) 00675-2.
[48] H. Calmet, A.M. Gambaruto, A.J. Bates, M. Vazquez, G. Houzeaux, D.J. Doorly, Large-scale CFD simulations of the transitional and turbulent regime for the large human airways during rapid inhalation, Comput. Biol. Med. 69 (2016) 166–180.
[49] J.M. Oakes, A.L. Marsden, C. Grandmont, C. Darquenne, I.E. Vignon-Clementel, Distribution of aerosolized particles in healthy and emphysematous rat lungs: Comparison between experimental and numerical studies, J. Biomech. 48 (2015) 1147–1157.
[50] S.J. Sherwin, V. Franke, J. Peiro, K. Parker, One-dimensional modelling of a vascular network in space–time variables, J. Eng. Math. 47 (2003) 217–250.
[51] L. Formaggia, A. Quateroni, A. Veneziani, Cardiovascular Methamatics – Modeling and Simulation of the Circulatory System, Springer-Verlag, Italia, Milano, 2009.
[52] J. Mead, T. Takishima, D. Leith, Stress distribution in lungs: a model of pulmonary elasticity, J. Appl. Physiol. 28 (1970) 596–608.
[53] T. Pedley, R. Schroter, M. Sudlow, The prediction of pressure drop and variation of resistance within the human bronchial airways, Respir. Physiol. 9 (1970) 387–405.
[54] D. Reynolds, J. Lee, Modeling study of the pressure-flow relationship of the bronchial tree (abstract), FASEB J. 38 (1979) 1444.
[55] G.F. Nieman, L.A. Gatto, N.M. Habashi, The impact of mechanical ventilation on the pathophysiology of progressive acute lung injury, J. Appl. Physiol. 119 (2015) 1245–1261.
[56] M.H. Tawhai, A.H. Pullan, P.J. Hunter, Generation of an anatomically based three-dimensional model of the conducting airways, Ann. Biomed. Eng. 28 (2000) 793–802.

[57] E.R. Weibel, Morphometry of the Human Lung, Springer, Berlin-Göttingen-Heidelberg, Germany, 1963.
[58] E. Weibel, The Pathway for Oxygen: Structure and Functiona in Mammalian Respiratory System, Harvard University Press, Cambridge, Massachusetts, USA, 1984.
[59] A. Majumdar, A. Alencar, S. Buldyrev, Z. Hantos, K. Lutchen, H. Stanley, B. Suki, Relating airway diameter distributions to regular branching asymmetry in the lung, Phys. Rev. Lett. 95 (2005) 168–201.
[60] R.J. Metzger, O.D. Klein, G.R. Martin, M.A. Krasnow, The branching programme of mouse lung development, Nature 453 (2008) 745–750.
[61] C. van Ertbruggen, C. Hirsch, M. Paiva, Anatomically based three-dimensional model of airways to simulate flow and particle transport using computational fluid dynamics, J. Appl. Physiol. 98 (2005) 970–980.
[62] J.H.T. Bates, C.G. Irvin, Time dependence of recruitment and derecruitment in the lung: a theoretical model, J. Appl. Physiol. 93 (2002) 705–713.
[63] C.B. Massa, G.B. Allen, J.H.T. Bates, Modeling the dynamics of recruitment and derecruitment in mice with acute lung injury, J. Appl. Physiol. 105 (2008) 1813–1821.
[64] B. Ma, J.H.T. Bates, Modeling the complex dynamics of derecruitment in the lung, Ann. Biomed. Eng. 38 (2010) 3466–3477.
[65] H.D. Prange, Laplace's law and the alveolus: a misconception of anatomy and a misapplication of physics, Adv. Physiol. Educ. 27 (2003) 34–40.
[66] D. Talmor, T. Sarge, A. Malhotra, C.R. O'Donnell, R. Ritz, A. Lisbon, V. Novack, S.H. Loring, Mechanical ventilation guided by esophageal pressure in acute lung injury, N. Engl. J. Med. 359 (2008) 2095–2104.
[67] C.J. Roth, T. Becher, I. Frerichs, W.A. Wall WA, Coupling EIT and a computational lung model for predicting patient-specific ventilatory response, in: J. Sola, F. Braun, A. Adler (Eds.), Proceedings of the 16th International Conference on Biomedical Applications of Electrical Impedance Tomography, Neuchatel, Switzerland, 2015, p. 80.
[68] A. Protti, M. Cressoni, A. Santini, T. Langer, C. Mietto, D. Febres, M. Chierichetti, S. Coppola, G. Conte, S. Gatti, O. Leopardi, S. Masson, L. Lombardi, M. Lazzerini, E. Rampoldi, P. Cadringher, L. Gattinoni, Lung stress and strain during mechanical ventilation: any safe threshold? Am. J. Respir. Crit. Care Med. 183 (2011) 1354–1362.
[69] B. Suki, A.L. Barabasi, Z. Hantos, F. Petak, H.E. Stanley, Avalanches and power-law behaviour in lung inflation, Nature 368 (1994) 615–618.
[70] B.H. Brown, Electrical impedance tomography (EIT): a review, J. Med. Eng. Technol. 27 (2003) 97–108.
[71] A. Adler, J.H. Arnold, R. Bayford, A. Borsic, B. Brown, P. Dixon, T.J.C. Faes, I. Frerichs, H. Gargnon, Y. Gärber, B. Grychtol, G. Hahn, W.R.B. Lionheart, A. Malik, R. Patterson, J. Stocks, A. Tizzard, N. Weiler, G.K. Wolf, GREIT: a unified approach to 2d linear EIT reconstruction of lung images, Physiol. Meas. 30 (2009) S35–S55.
[72] P. Nopp, E. Rapp, H. Pfützner, H. Nakesch, C. Ruhsam, Dielectric properties of lung tissue as a function of air content, Phys. Med. Biol. 38 (1993) 699–716.
[73] P. Nopp, N.D. Harris, T.-X. Zhao, B.H. Brown, Model for the dielectric properties of human lung tissue against frequency and air content, Med. Biol. Eng. Comput. 35 (1997) 695–702.
[74] C.J. Roth, A. Ehrl, T. Becher, I. Frerichs, J.C. Schittny, N. Weiler, W.A. Wall, Correlation between alveolar ventilation and electrical properties of lung parenchyma, Physiol. Meas. 36 (2015) 1211–1226.
[75] I. Frerichs, Electrical impedance tomography (EIT) in applications related to lung and ventilation: a review of experimental and clinical activities, Physiol. Meas. 21 (2000) R1-21.
[76] M.S. Olufsen, C.S. Peskin, W.Y. Kim, E.M. Pedersen, A. Nadim, J. Larsen, Numerical simulation and experimental validation of blood flow in arteries with structured-tree outflow conditions, Ann. Biomed. Eng. 28 (2000) 1281–1299.
[77] M.I. Townsley, Structure and composition of pulmonary arteries, capillaries and veins, Compr. Physiol. 2 (2013) 675–709.
[78] J.S. Brody, E.J. Stemmler, A.B. Dubois, Longitudinal distribution of vascular resistance in the pulmonary arteries, capillaries, and veins, J. Clin. Invest. 47 (1968) 783–799.
[79] C.D. Murray, The physiological principle of minimum work applied to the angle of branching of arteries, J. Gen. Physiol. 9 (1926) 835–841.
[80] J. Valentin, Basic anatomical and physiological data for use in radiological protection: reference values: {ICRP} publication 89, Ann. {ICRP} 32 (2002) 1–277.
[81] J. Keener, J. Sneyd, Mathematical Physiology, Springer Verlag, 1998.
[82] E.R. Weibel, Symmorphosis: On Form and Function in Shaping Life, Harvard University Press, 2000.
[83] J.B. West, Respiratory Physiology: The Essentials, Lippincott Williams and Wilkins, 2008.
[84] M. Ismail, Reduced dimensional modeling of the entire lung (Ph.D. thesis), Technische Universität München, 2014.
[85] A.C. Guyton, J.E. Hall, Medical Physiology, Elsevier Saunders, 2005.
[86] J.S. Brody, E.J. Stemmler, A.B. Dubois, Longitudinal distribution of vascular resistance in the pulmonary arteries, capillaries, and veins, J. Clin. Invest. 47 (1968) 783–799.
[87] A.C.I. Malossi, P.J. Blanco, S. Deparis, A two-level time step technique for the partitioned solution of one-dimensional arterial networks, Comput. Methods Appl. Mech. Engrg. 237 (2012) 212–226.
[88] D. Chemla, V. Castelain, M. Humbert, J.L. Hébert, G. Simonneau, Y. Lecarpentier, P. Hervé, New formula for predicting mean pulmonary artery pressure using systolic pulmonary artery pressure, Chest 126 (2004) 1313–1317.
[89] M. Denny, Air and Water: The Biology and Physics of Life's Media, Princeton University, 1993.
[90] G. Thews, Die Sauerstoffdiffusion in der Lunge. Ein Verfahren zur Berechnung der O2 Diffusionszeiten, der Kontaktzeit und des O2-Diffusionsfaktors, Pflüger's Arch. 265 (1957) 154–171.
[91] R. Harris, Pressure-volume curves of the respiratory system, Respir. Care 50 (2005) 78–99.
[92] A.S. Slutsky, J.M. Drazen, R.H. Ingram, R.D. Kamm, A.H. Shapiro, J.J. Fredberg, S.H. Loring, J. Lehr, Effective pulmonary ventilation with small-volume oscillations at high frequency, Science 209 (1980) 609–671.
[93] S. Martin, B. Maury, Modeling of the oxygen transfer in the respiratory process, ESAIM Math. Model. Numer. Anal. 47 (2013).